Journal Name

ARTICLE TYPE

Cite this: DOI: 00.0000/xxxxxxxxxx

Nitrogen substitutional defects in Silicon. A quantum mechanical investigation of the structural, electronic and vibrational properties.

Alexander Platonenko,[a] Francesco Silvio Gentile,[b] Fabien Pascale,[c] Anna Maria Ferrari,[a] Maddalena D'Amore,[a] and Roberto Dovesi[a]

Received Date
Accepted Date

DOI: 00.0000/xxxxxxxxxx

The vibrational Infrared (IR) and Raman spectra of seven substitutional defects in bulk silicon are computed, by using the quantum mechanical CRYSTAL code, the supercell scheme, an *all electron* Gaussian type basis set and the B3LYP functional. The relative stability of various spin states has been evaluated, the geometry optimized, the electronic structure analyzed. The IR and Raman intensities have been evaluated analitically. In all cases the IR spectrum is dominated by a single N peak (or by two or three peaks with very close wavenumbers), whose intensity is at least 20 times larger than the one of any other peak. These peaks fall in the 645-712 cm^{-1} interval, and a shift of few cm^{-1} is observed from case to case. The Raman spectrum of all defects is dominated by an extremely intense peak at about 530 cm^{-1}, resulting from the (weak) perturbation of the peak of pristine silicon.

1 Introduction

Nitrogen in silicon is known to improve material properties in various ways, increasing mechanical strength and greatly reducing the size and density of void defects.[1–3] It was observed that nitrogen increases precipitation of oxygen by increasing the number of nucleation sites and retarding silicon self-interstitial migration.[4] N impurities can pin dislocations[5] and form electrically active defects such as the substitutional deep donor.[6]

A photoluminescence zero-phonon at 1.223 eV, also known as "A,B,C", has been correlated with nitrogen content in doped silicon.[7,8] It appears after annealing at 1000 K and has been attributed to a diamagnetic defect; it is believed that a couple of nitrogen atoms form a complex defect.

Nitrogen can be introduced into Si by adding Si_3N_4 to the Si melt, annealing in an atmosphere of N_2 or NF_3.[9,10] Diffusivity of the N-N pair was found to be three orders of magnitude higher than the oxygen one at 1100 K.[11] Nitrogen solubility in silicon is however very small, so concentration of natural N defects is usually low, making experimental measurements difficult.

Silicon with high N content can however be obtained through implantation techniques and subsequent pulsed laser annealing.[12] This increased concentration of N atoms permits accurate IR measurements. Stein's IR spectra,[13,14] obtained along these lines, present characteristic peaks at 551, 653, 687, 766 and 963 cm^{-1}. Quantum mechanical simulations are obviously the natural alternative to experiment, in particular when the latter is difficult due to low N concentration, or other reasons.

An extensive simulation of the vibrational properties of various defects in silicon has been performed about 15 years ago by Goss *et al.*,[15] by using a quantum-mechanical approach, Gaussian type functions and pseudopotentials, a GGA type functional and a supercell scheme. Geometry, charge distribution and vibrational frequencies are reported. The latter will be compared with the ones of the present study. The main limitation of the very rich and inspiring investigation by Goss *et al.* is that only the vibrational frequencies are produced, but not the IR and Raman intensities, so that no indication at all is provided concerning the number of important peaks that should appear in the spectrum, their relative intensity, and then their correlation with the presence of various possible defects.

In the present paper we characterize seven N substitutional defects (see Figure 1) on the basis of the vibrational IR and Raman spectra. We underline that for the first time the IR and Raman intensities are presented, and that they are computed analytically. In a parallel paper[16]the analysis is extended to eight interstitial or more complex defects.

The first analyzed defect is the single substitutional nitrogen, in-

[a] *Institute of Solid State Physics, University of Latvia, 8 Kengaraga street, LV1063, Riga, Latvia*

[b] *Dipartimento di Chimica, Università di Torino and NIS (Nanostructured Interfaces and Surfaces) Centre, Via P. Giuria 5, 10125 Torino, Italy*

[c] *Université de Lorraine – Nancy, CNRS, Laboratoire de Physique et Chimie Théoriques, UMR 7019. Vandœuvre-lès-Nancy, 54506 France*

† Electronic Supplementary Information (ESI) available: [details of any supplementary information available should be included here]. See DOI: 00.0000/00000000.

dicated as N_s (top left panel of Figure 1), that leaves one uncoupled electron on one of its first neighbors. The N_s-N_s defect (top righ panel), with a double substitution of two vicinal silicon atoms, has also been analyzed. We investigated then the four VN_x defects (bottom left), in which one to four (x=1 to 4) silicon atoms around the vacancy are substituted by a nitrogen atom. V_2N_2, two nitrogen atoms sitting close the two vicinal vacancies, has also been explored (bottom right). Among the possible relative positions, we considered the one in which the two nitrogen atoms are on the border of one of the two vacancies. In standard conditions all the above defects appear, to our knowledge, in the neutral charge state. This kind of substitution (N for Si around the vacancy) is very favorable, as one silicon atom bearing one uncoupled electron is replaced by a nitrogen atom able to form only three covalent bonds. Moreover, the vacancy offers the space for allocating the lone pairs of the nitrogen atoms. Besides the IR and Raman spectra, the equilibrium geometry, the relative stability of the possible spin states, the charge and spin (when applies) densities, as well as the band structure of the various systems are provided.

The paper is structured as follows. Section 2 contains the details of the computational procedures and conditions. Section 3 is organized in three parts: subsection 3.1 describes the fully-relaxed structures of the defective lattices, their charge (and spin) distributions and band structures; subsection 3.3 reports the corresponding vibrational features and their detailed analysis, whereas in subsection 3.2 the formation energies are presented. A discussion of the present results, with a comparison with the (few) experimental results and previous calculations is presented in section 4. A few conclusions are drawn in Section 5.

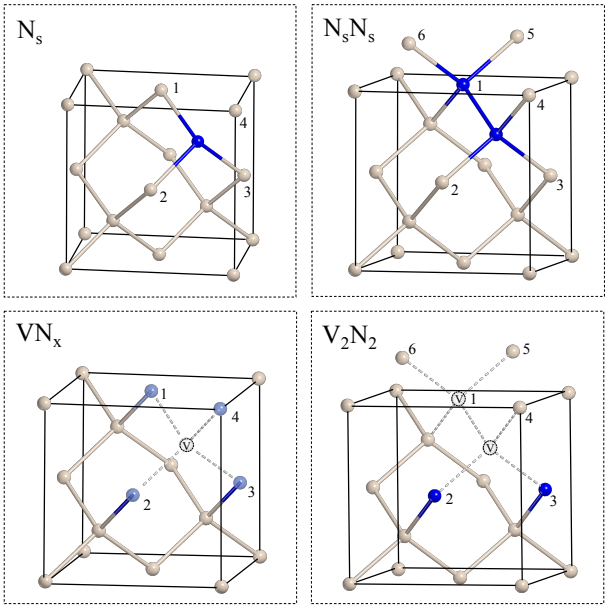

Fig. 1 Schematic representation of the seven N substitutional defects here investigated. The four VN_x defects are obtained, in the left-bottom panel, substituting 1 to 4 carbon atoms around the vacancy with nitrogen atoms (depicted with translucent blue color). Note in V_2N_2 the two vicinal vacancies, and that the two N atoms are close to the same vacancy.

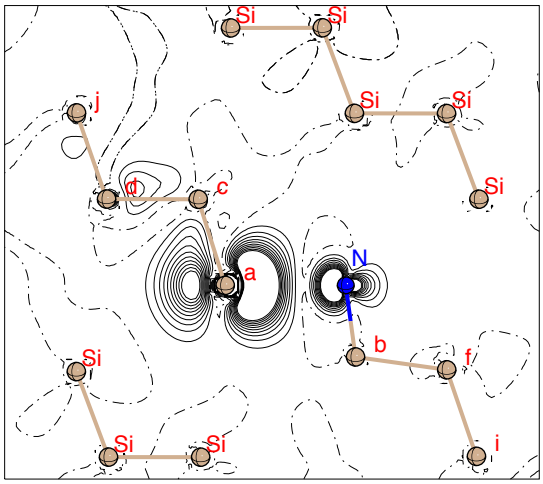

Fig. 2 Spin density map of substitutional nitrogen in silicon. The plane of the figure is defined by atoms Si_a, N and Si_b (see labels a and b in figure 1). Isodensity lines differ by 0.01 $|e|$ $(a_0)^{-3}$. Spin density is truncated at $\pm$ 0.1 | e | $(a_0)^{-3}$. Continuous, dashed and dot-dashed black lines indicate positive, negative and zero values, respectively.

2 Computational Details

Calculations have been performed by use of the B3LYP global hybrid functional,[17,18] as implemented in the CRYSTAL17 program.[19] As nitrogen, at variance of silicon, that is fourfold coordinated, is able to bind to only three neighbors, in many cases there are unpaired electrons in the unit cell. For these cases an open shell solution was looked for, by using the Spin Unrestricted Kohn-Sham DFT options available in CRYSTAL.[19] An *all-electron* Gaussian type basis set (derived from Pople's standard 6-21G[20]) as described in D'Arco *etal*.[21] has been adopted for silicon: the contraction is 6-5111G* (22 atomic orbitals, AOs), where the first contraction is of *s* type, followed by 4 *sp* and one d shell; the exponents of the two outermost *sp* shells have been set to 0.45 and 0.15 Bohr^{-2}, respectively. For the nitrogen atom, the 6-31G*[22] contraction has been adopted without modifications (14 AOs).

The truncation of the Coulomb and exchange infinite lattice series is controlled by five thresholds T_i (see CRYSTAL manual, Ref.23, for more details), which have been set to 8 (T_1-T_4) and 16 (T_5). The convergence threshold on energy for the self-consistent-field (SCF) procedure has been set to 10^{-8} Ha for the structural optimization, and to 10^{-11} Ha for the vibration calculations.

The DFT exchange-correlation contribution to the Fock matrix has been evaluated by numerical integration over the unit cell volume. Radial and angular points for the integration grid are generated through Gauss-Legendre radial quadrature and Lebedev two-dimensional angular point distributions. The default pruned grid with 99 radial and 1454 angular points has been used, whose accuracy can be measured by comparing the integrated charge density in the largest supercell here considered (216 atoms) for the substitutional defect, $N_i = 3012.011$, with 3012, the total number of electrons in the unit cell.

system	q_N	μ_N	R_{N-Si}	q_{Si_N}	μ_{Si_N}	q_{Si_O}	μ_{Si_O}	$R_{Si_O-Si'}$	$q_{Si'}$	$\mu_{Si'}$	ΔE
N_s	-1.026	+0.063	1.866	+0.400	0.008	+0.024	+0.732	2.331	-0.012	-0.007	
VN_1^q	-1.043	+0.018	1.860	+0.412	0.005	+0.009	+0.785	2.335	-0.011	0.003	0.78
VN_1^d	-1.047	+0.003	1.848	+0.414	-0.001	+0.007	+0.443	2.342	-0.012	0.028	0.0
	-	-	-	-	-	+0.020	-0.180	2.377	-0.011	-0.040	
VN_2^t	-1.045	+0.012	1.849	+0.413	0.005	+0.014	+0.779	2.319	-0.013	0.002	0.92
VN_2^s	-1.050	0.000	1.840	+0.414	0.000	+0.017	0.000	2.367	-0.010	0.000	0.0
VN_3^d	-1.047	+0.006	1.839	+0.414	0.004	+0.013	+0.777	2.320	-0.013	-0.006	
VN_4^s	-1.048	0.00	1.834	+0.419	0.00	-	-	-	-	-	
N_s-N_s	-1.043	0.00	1.844	+0.416	0.00	-	-	-	-	-	
$V_2N_2^Q$	-1.045	+0.011	1.847	+0.410	+0.007	+0.010	+0.795	2.322	-0.021	+0.003	1.01
$V_2N_2^{t1}$	-1.045	-0.001	1.847	+0.410	+0.010	+0.016	+0.795	2.332	-0.012	+0.054	0.93
$V_2N_2^{t2}$	-1.046	+0.078	1.841	+0.410	+0.006	-0.009	+0.697	2.319	-0.015	-0.004	0.02
$V_2N_2^s$	-1.046	+0.006	1.841	+0.410	+0.004	-0.009	-0.687	2.317	-0.024	+0.005	0.0

Table 1 Atomic net charges q and magnetic moments μ (in $|e|$) of the atoms around the N_s and N_s-N_s defects, and around the vacancy in the VN_x (x = 1 to 4) and V_2N_2 defects, and distances R (in Å). Si_N, Si_O and Si' are the Si atoms linked to N, the Si atoms opposite to N, and the Si atoms linked to the Si atom opposite to N. Superscripts Q, q, t, d, s stand for quintuplet, quadruplet, triplet, doublet, singlet. See text for the definition of the two triplet states of V_2N_2. ΔE is the energy difference in eV between the spin states as obtained with the S_{64} supercell. In the VN_1^d case the 3 carbon atoms around the vacancy are not equivalent: their data are reported in two subsequent lines.

A periodic super-cell approach is used to simulate different defect concentrations. Cubic super-cells containing 64 and 216 atoms have been considered (to be referred to in the following as S_n, with n= 64 or 216). They correspond to the expansion of the bulk silicon conventional cell, containing 8 atoms, by a factor 2 and 3 along the three lattice parameters. The various defects reduce the symmetry, that for the substitutional case is C_{3v}; the deformation of the cell from the cubic shape is negligible. Overall, the size of the basis set (number of AOs) is 1400 in S_{64} and 4744 in S_{216}. Reciprocal space has been sampled using a regular sub-lattice with a shrinking factor of 4 for S_{64} and of 2 for S_{216} which correspond to a sampling over 13 and 4 **k**-points in the irreducible part of the Brillouin zone for the substitutional defect of C_{3v} point-symmetry.

2.1 Harmonic frequencies and the IR and Raman spectra

Frequencies at the Γ point are obtained within the harmonic approximation by diagonalizing the mass-weighted Hessian matrix, W, whose elements are defined as [24–28]

$$W^{\Gamma}_{\alpha i,\beta j} = \frac{H^{\mathbf{0}}_{\alpha i,\beta j}}{\sqrt{M_\alpha M_\beta}} \quad \text{with} \quad H^{\mathbf{0}}_{\alpha i,\beta j} = \left(\frac{\partial^2 E}{\partial u^{\mathbf{0}}_{\alpha i} \partial u^{\mathbf{0}}_{\beta j}} \right), \qquad (1)$$

where M_α and M_β are the masses of atoms associated with the i and j atomic coordinates. Once the Hessian matrix, $H^{\mathbf{0}}_{\alpha i,\beta j}$, has been calculated, frequency shifts due to isotopic substitutions can be calculated readily, at no computational cost, by changing masses in Equation 1.

Energy first derivatives with respect to the atomic displacements, $v_{\alpha,j} = \partial E \big/ \partial u_{\alpha,j}$, are calculated analytically for all the $u_{\alpha,j}$ coordinates (E is the total energy, $u_{\alpha,j}$ is the displacement coordinate with respect to equilibrium, α labels each atom), whereas second order derivatives at the equilibrium geometry are calculated

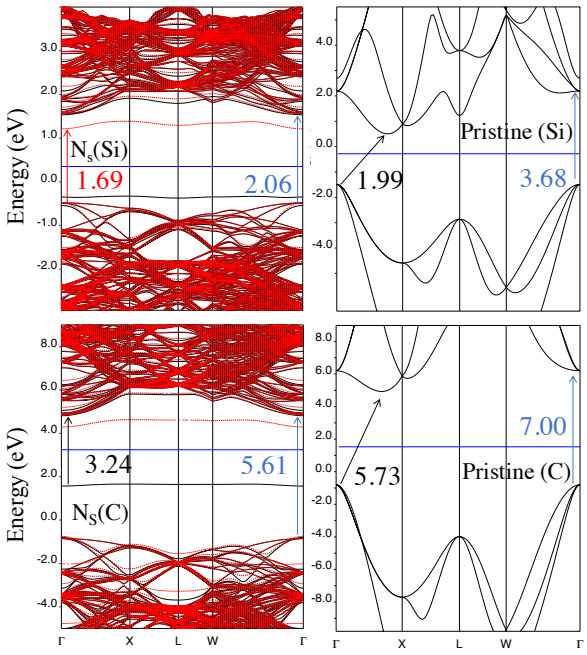

Fig. 3 Band structure of substitutional N in silicon (top, left) and diamond (bottom, left). To the right, the band structure of pristine bulk silicon (top) and diamond (bottom) are shown, for comparison. In all defective cases the S_{216} supercell has been used, while for the pristine silicon the primitive cell has been adopted. The blue lines is the Fermi level. The direct (at the Γ point) and indirect band gap of perfect silicon are reported. For the defective system, the red arrow indicates the gap between the top of the valence band and the empty defect level. Gaps in eV.

numerically using a single displacement along each coordinate:

$$\left[\frac{\partial v_{\alpha j}}{\partial u_{\beta i}}\right] \approx \frac{v_{\alpha j}(0,\ldots,u_{\beta i},\ldots,0) - v_{\alpha j}(0,\ldots,0,\ldots,0)}{u_{\beta i}} \quad (2)$$

Previous calculations[24,29] have shown that in bulk systems the influence of u is very small (less than 1 cm^{-1}) when H atoms are not present. Integrated intensities for IR absorption $\mathscr{I}_p$ are computed for each mode p by means of the mass-weighted effective-mode Born-charge vector $\vec{Z}_p$[30,31] evaluated through a CPKS approach:[32,33]

$$\mathscr{I}_p \propto \left|\vec{Z}_p\right|^2 . \quad (3)$$

The relative Raman intensities of the peaks are computed analytically by exploiting a scheme illustrated in refs.34,35. Both schemes are based on the solutions of first- and second-order Coupled-Perturbed-Kohn-Sham equations.[36,37]

3 Results.

3.0.1 Electronic structure and spin states.

In N_s, nitrogen binds to three neighbors, the fourth one is carrying formally one uncoupled electron. We will discuss in the following the amount of localization of this electron on the silicon atom. The state is then a doublet d, with S_z=1/2. It is a doublet also in the VN_3 defect, with three nitrogen atoms around the vacancy. The remaining silicon atom has an unpaired electron. VN_4 and N_s-N_s are closed shell systems. In VN_1 and VN_2 there are respectively 3 and 2 unpaired electrons around the vacancy. In both cases there are two possible states: quadruplet q (S_z=3/2) and doublet d (S_z=1/2) in the first case, triplet t (S_z=1) and singlet s (S_z=0) in the second. In V_2N_2 (two nitrogen atoms around two vicinal vacancies, both on the same side) there are four unpaired electrons, and the possible spin states are a quintuplet Q (S_z=2), two triplets (S_z=1; the spin down electron can be on the side of the two nitrogen atoms, or on a silicon atom sitting around the vacancy with no nitrogen atoms) and a singlet. The equilibrium total electronic energy and geometry and the vibrational IR and Raman spectra of these twelve states have been investigated. The essential information is summarized in Tables 1 and 3.

3.1 Geometry, charge and spin densities, and band structure.

3.1.1 N_s

Fig. 1, top left, shows the N_s defect in the conventional cell of bulk silicon. The defect reduces the point symmetry from T_d to C_{3v}. The N-Si distance is as short as 1.87 Å, to be compared to 2.37 Å for the Si-Si distance in pristine silicon. The nitrogen atom is nearly sitting on the plane defined by its three neighbors, the distance from the center of the Si triangle being only 0.25 Å. The Si-N-Si angle is 118.2°. The distance to the fourth silicon neighbor, the one bearing the uncoupled electron, is as large as 3.11 Å, due to both the N lone pair (oriented along the C_{3v} axis) steric hindrance and the electrostatic repulsion between the latter and the unpaired electron.

The net charge on the N atom, obtained from a Mulliken analysis, is -1.026 $|e|$; it is overcompensated by the +0.400 $|e|$ on the three equivalent $Si_{(b)}$ atoms; slightly negative net charges on first and second neighbors of these $Si_{(b)}$ atoms dump the charge oscillations, that on farther neighbors of N are essentially null. On the opposite side of the N defect, the $Si_{(a)}$ atom and its neighbors are nearly neutral. The N-$Si_{(b)}$ bond population is large and positive (+0.201 $|e|$), indicating a medium covalent character of the bond. This value is smaller than the Si-Si one in bulk silicon, that is +0.328 $|e|$. The N-$Si_{(a)}$ bond population is very close to zero and negative (-0.004 $|e|$) indicating an antibonding character of the interaction.

It is interesting to explore how much the uncoupled electron is localized on the $Si_{(a)}$ atom, and how far the spin density wave propagates along the covalent network. The atomic magnetic moments μ, obtained from a Mulliken partition of the spin density, are shown in Figure 1. Most of the spin density is localized on the $Si_{(a)}$ atom, with μ= 0.732 $|e|$; the second most important contribution is on the N atom (0.063 $|e|$). These numbers are extremely close to the ones reported by Brower[38] as a result of the analysis of the experimental EPR data (73% of the uncoupled electron on $Si_{(a)}$ and 7% on N). The remaining fraction of the unpaired electron (0.205 $|e|$) is on farther neighbors, the largest contributions (overall 0.134 $|e|$, bringing the total to 0.929 $|e|$) coming from the two $Si_{(d)}$ atoms (0.037x2 $|e|$) and the three $Si_{(j)}$ atoms (0.020x3 $|e|$).

The spin density map (Fig. 2) through the plane defined by the $Si_{(c)}$, $Si_{(a)}$ and N atoms confirms the above data, *i.e.* that most of the spin density is localized on the $Si_{(a)}$ atom; note the p type shape of the density. A similar (but much smaller) p type spin polarization is observed also on N, whereas the spin density on all other atoms of the unit cell is very close to zero.

Figure 3 compares the band structure of the N substitutional defect in silicon (top left) and diamond (bottom left). The latter is also known as the C defect. To the right of the figure, the band structure of pristine silicon (top) and diamond (bottom) are also shown, for illustrating the effect of the defect on perfect bulk.

Note that the pristine silicon ground state is a closed shell, while the defect ground state is an open shell structure (a doublet state, S_z=1/2, due to the uncoupled electron on the Si or C atom opposite to N). The blue horizontal line indicates the Fermi level, conventionally located midway between the top of the valence band and the bottom of the conduction band of the pristine system. Perfect diamond has a computed band gap of 5.73 eV (it is a large gap insulator); perfect silicon is a semiconductor with an indirect band gap of 1.99 eV and a direct gap at Γ of 2.38 eV. In diamond (silicon), the energy difference between the occupied defect level, that is about 2.32 (0.13) eV above the top of the valence band, and the empty defect level, that is 0.54 (0.34) eV below the bottom of the conduction band, is 2.75 (1.53) eV.

3.1.2 VN_x, V_2N_2 and N_s-N_s.

The analysis of the charge and spin distribution of the other cases will be more synthetic than the one performed for N_s. Table 1 provides however the essential information for understanding the IR and Raman spectra to be discussed in the next section.

In short:

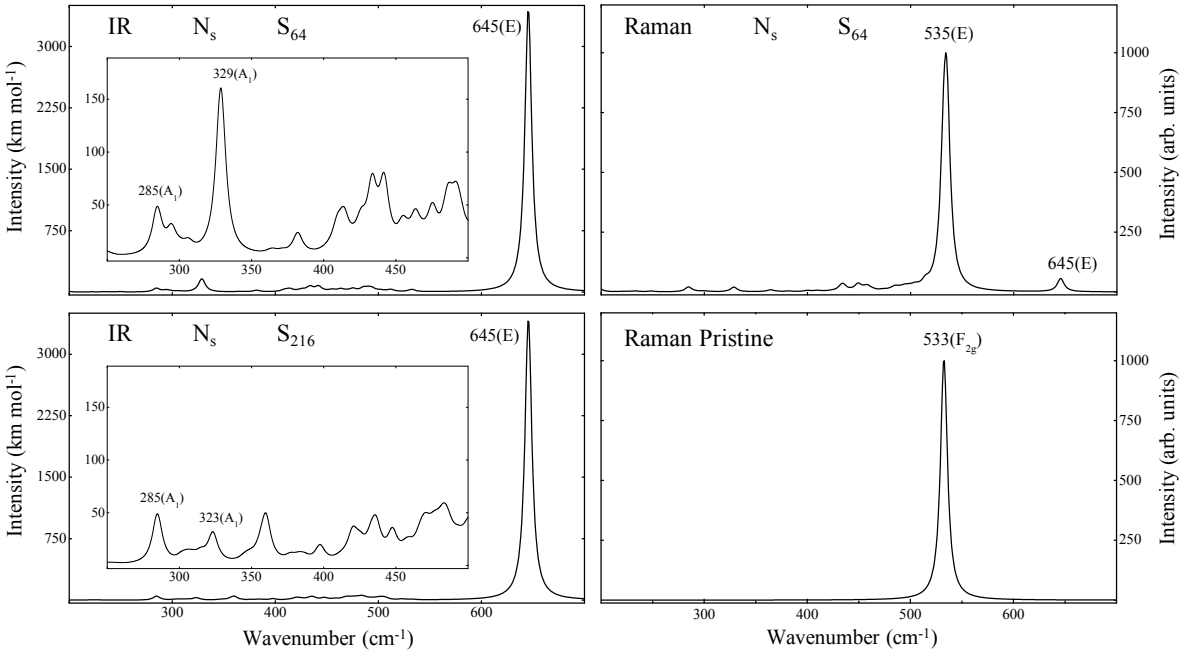

Fig. 4 Top: simulated IR (left) and Raman (right) spectrum of the substitutional N_s defect in silicon obtained with S_{64}. Bottom: to the left, the IR spectrum obtained with S_{216}. To the right, the Raman spectrum of pristine silicon. A Lorentzian function with FWHM of 8 cm^{-1} has been used for the convolution of the eigenvalues.

Method	E_D (Ha)	E_f^1 (eV)	E_f^1/N (eV)	E_f^2 (eV)	E_f^2/N (eV)
N_s	-18291.15276	1.96	1.96	-2.75	-2.75
N_s-N_s	-18056.45807	0.90	0.45	-8.54	-4.27
VN_1^d	-18001.61733	3.79	3.79	-0.92	-0.92
VN_2^s	-17766.92349	2.71	1.35	-6.73	-3.36
VN_3^d	-17532.19913	2.45	0.82	-11.70	-3.90
VN_4	-17297.51532	1.09	0.27	-17.78	-4.44
$V_2N_2^s$	-17477.36100	5.27	2.64	-4.16	-2.08

Table 2 Formation energy E_f^1 (in eV) of the substitutional defects in silicon (see equation 4), computed with reference to the N_2 molecule and the perfect silicon bulk total energies. Data refer to the silicon supercell containing 64 atoms before the defect formation. The total energy of the S_{64} perfect silicon supercell is -18525.95870 Ha (-289.46811 Ha per atom). The energy of the N_2 molecule is -109.46852 Ha (54.73426 Ha per atom). E_f^2 is the formation energy evaluated with respect to the isolated atoms, and differs from E_f^1 by 4.72 eV per nitrogen atom (half the N_2 binding energy).

a) The Table shows that the low spin state is by far the most stable one: by 0.78 eV for VN_1, by 0.92 for VN_2. In the V_2N_2 case, one of the two possible triplet states (the one with the spin down on one of the three silicon atoms sitting around the vacancy without nitrogen atoms) has energy just above the singlet one. This means that the subsequent analysis could be limited to VN_1^d, VN_2^s and $V_2N_2^s$. However, in order to be able to explore the influence of the spin state on the IR and Raman spectra, we will compare the high and low spin states in the following. Additional data for the high spin states are reported in the Supplementary Material Section (SMS).

b) When comparing the various columns referring to N in Table 1 (left part of the Table), we observe that all reported quantities change by very small amounts in going from a defect to the other: for example q_N, the Mulliken net charge of nitrogen, varies from -1.026 (N_s) to -1.050 $|e|$ (NV_2^s); the net charge of the three silicon atoms linked to N, vary from +0.400 $|e|$ (N_s) to +0.419 $|e|$ (N_4). The distance between N and its first neighbors varies from 1.834 Å(VN_4) to 1.869 Å(N_s).

As regards the atomic spin momentum μ, it is always quite small on N (the largest value is +0.06 $|e|$ in N_s, much smaller in the other cases). The magnetic moment on the three silicon atoms linked to N is even smaller, the largest value being +0.008 $|e|$, again in N_s. In summary, the difference for the same quantity in different defects is always very small. The two systems showing extreme values are N_s and VN_4.

Let us consider now the opposite side with respect to N, whose data are shown in the right part of the Table. Here the situation can be different from case to case. The VN_4 and N_s-N_s defects are symmetric (N atoms and their neighbors as described in the left side). In the N_s case, Si_O is the silicon atom with the uncoupled electron, as described above. In the VN_x cases (x=1 to 3), Si_O are the Si atoms (3, 2 or 1, respectively) sitting around the vacancy, and Si' are the silicon atoms linked to Si_O. The same applies to V_2N_2.

The q_{Si_O} charges are extremely small, being these atoms not directly linked to N. They are slightly positive (the influence of N is not completely absent), and are compensated by the even smaller and negative $q_{Si'}$ charges of the silicon atoms on the back with respect to the defect. The $R_{Si_O-Si'}$ distances are very similar in all cases, (they span from 2.32 to 2.38 Å), and close to the Si-Si distance in bulk silicon, 2.37 Å, so the interesting part of the Table are the μ_{Si_O} data, that provide information on the more or less localized nature of the uncoupled electrons (if any). The momentum μ_{Si_O} in the four high spin cases is about the same: +0.732 in N_s, +0.785 in VN_1^q, +0.779 in VN_2^t and +0.777 $|e|$ in VN_3. In the VN_1^d doublet it is much lower, +0.443 $|e|$ on two Si atoms around the vacancy, and -0.180 $|e|$ on one of them. So overall the three Si_O atoms are carrying +0.706 $|e|$ out of the total of one unpaired electron The remaining +0.294 $|e|$ are spread over farther neighbors.

The $\mu_{Si'}$ values are much smaller than the μ_{Si_O} ones, the largest value being -0.04 $|e|$ (in most cases positive and negative μ values alternate along the chains of neighbors). The band structure of many of the defects are shown in the Supplementary Material Section, with some short comments.

3.2 Formation Energy.

Defect formation energies E_f were calculated according to the following equation:

$$x\mathrm{Si} - (v+y)\mathrm{Si} + y\mathrm{N}^i \overset{\mathrm{E}_f}{\rightleftharpoons} \mathrm{Si}_{(x-y-v)}\mathrm{N}_y \qquad (x = 64,216; \quad y = 1,2,3,4; \quad v = 0,1,2) \tag{4}$$

where $\mathrm{Si}_{(x-y-v)})\mathrm{N}_y$ is the defective system containing $x-y-v$ atoms, whose energy will be indicated as E_D, xSi is the perfect bulk supercell containing x atoms (E_P is its energy, with $E_P = x\mathrm{E}_{Si}$), y is the number of substituted nitrogen atoms, and v the number of vacancies. This corresponds to extract from the perfect supercell $v+y$ Si atoms and to add y N atoms. The E_f formation energy reads:

$$E_f^i = E_D - (x-y-v)E_{Si} + yE_N^i \tag{5}$$

As regards the definition of E_N, we have followed two different approaches, denoted by superscripts 1 and 2. In the first one (E_f^1), E_N is half the energy of the N_2 molecule (-54.73426 Ha), i.e. the most stable form of elemental nitrogen.

Table 2 reports E_f^1, and E_f^1/N, *i.e.* the formation energy per nitrogen atom. In the second definition, E_f^2 is the formation energy evaluated with respect to the isolated nitrogen atom. The difference between the two is obviously nothing else than the binding energy of the N_2 molecule (0.35276 Ha/2). So the column E_f^2/N in Table 2 differs from E_f^1/N by the constant value of 4.72 eV (half the binding energy of N_2). This second definition might be useful when the nitrogen atom is supposed to be already present in the silicon bulk in atomic form. In this case it might be useful to know how the nitrogen orbitals extends over the basis set of the neighboring atoms of the unit cell, that is how large is the Basis Set Superposition Error (BSSE), that has been estimated by using the Counterpoise Method:[39]. The nitrogen atom has been surrounded by two shells of neighboring ghost atoms (no electrons, no nucleus, just the basis set is kept), located as in the pristine silicon structure. With this augmented basis set the atomic energy reduces by about 0.1 eV. As N_2 is a very stable molecule, in all cases E_f^1 is positive (endothermic process). The sign is reversed, on the contrary, it reference is done to the isolated nitrogen atoms.

The formation energy of a single silicon vacancy obtained from our model is about 4.7 eV (the experimental estimated value is 4.0 eV.)[40] If we subtract this quantity to the formation energies of the V_xN_y defects, we have a measure of the stabilizing effect of the nitrogen atoms sitting around the vacancy, as observed experimentally in N-doped Czochralski silicon. The formation energies of the single and double nitrogen substitutional defects here obtained are in quite good agreement with previously reported calculations (1.96 and 0.90 eV *vs.* 1.99 and 0.79 eV).[15]

It turns out that the VN_4 and N_s-N_s defects are very stable due to the closed shell structure, followed by VN_3 and VN_2.

3.3 Spectroscopic characterization.

The experimental Raman spectrum of pristine bulk silicon is very simple:[41] it is characterized by a single peak at 521 cm^{-1}; the calculated peak with the present functional and basis set is at 533 cm^{-1}, 12 cm^{-1} above (see the bottom right panel of Figure 4); we expect that all peaks of the spectrum be overestimated by about the same amount. The IR spectrum is even simpler: it is completely flat (no signal). So any observed IR peak, or any additional Raman peak must be attributed to one or more defects.

The analysis of the charge distribution (see previous subsection) confirms that the N-Si bond is very polar (the net charge of N is close to -1 $|e|$ in most of the cases); as a consequence, the defect atoms are expected to generate very intense IR peaks, that probably will dominate the spectrum. As the mass of nitrogen is nearly exactly half the one of silicon (14.01 vs 28.09 u), we can anticipate that many of the modes to which N contributes will appear well above the phonon band of pristine silicon, that has a calculated higher limit at 533 cm^{-1}.

The identification of the nature of the modes (which atom is contributing? what kind of movement is described by the mode?) can easily be performed through two tools implemented in the CRYSTAL code:

a) the isotopic shift (see the note following eq. 1); at negligible cost the mass of a subset of atoms can be altered arbitrarily. b)

Defect	Sym.	Modes	Int.
VN_1^q	C_{3v}	654 (E), 339 (A_1)	3630, 35
VN_1^d	C_s	664 (B"), 673 (A')	1782, 1689
VN_2^t	C_{2v}	675 (B_2), 677 (A_1), 667 (B_1)	3564, 2569, 1158
VN_2^s	C_2	693 (A'), 683 (A'), 674 (B")	3299, 2630, 1164
VN_3^d	C_{3v}	694 (A_1), 696 (E), 687 (E), 545 (E)	4844, 4002, 2080, 43
VN_4^s	T_d	712 (F_2), 535 (F_2), 552 (F_2)	14551, 108, 39
N_s^d	C_{3v}	645 (E), 329 (A_1)	3425, 160
$N_s - N_s^s$	C_{3v}	685 (E), 682 (E)	6854, 329
$V_2N_2^Q$	C_1	676 (A), 679 (A), 669 (A), 673 (A)	3235, 2698, 1253, 394
$V_2N_2^t$	C_1	688 (A), 694 (A), 671 (A), 686 (A)	2725, 2184, 1579, 775
$V_2N_2^s$	C_1	688 (A), 694 (A), 673 (A), 686 (A)	2675, 2255, 1550, 769

Table 3 Defect symmetry, wavenumbers of the most intense IR modes, with their symmetry and absolute intensities (in km/mol) are reported (in decreasing intensity order). Superscripts Q, q, t, d, s stand for quintuplet, quadruplet, triplet, doublet, singlet (S_z=2, 3/2, 1, 1/2 and 0, respectively). Data obtained with the S_{64} supercell.

the graphical animation of the modes. This permits to have a direct and clear evidence of the atoms and groups providing important contributions to the eigenvectors; it is available at the website *http://www.crystal.unito.it/animations-of-vibrational-modes.php*

3.3.1 The N_s IR spectrum

We discuss first the simple substitutional N_s spectrum, shown in the top left panel of figure 4, obtained with S_{64}.

If we consider the N atom as vibrating independently from the Si network (this is obviously a crude approximation, partially justified by the large mass difference between N and Si), on the basis of a simple symmetry analysis, we would expect the three N modes to have A_1 and E (doubly degenerate) symmetry. And actually the two dominant peaks at 645 (E symmetry) and 329 (A_1 symmetry) cm^{-1} correspond to a motion of the N atom along and perpendicular to the C_{3v} axis, as the graphical animation of the modes confirms. Note however that the intensity of the 645 cm^{-1} peak is about 20 times larger than the one at 329 cm^{-1}, that in turn is at least three times larger than any other peak in the spectrum. These peaks downshift by 5 cm^{-1} and 20 cm^{-1}, respectively, when ^{14}N is substituted by ^{15}N, confirming that they are nitrogen peaks. The comparison of the top and bottom left panels of Figure 4 shows how the IR spectrum evolves when the concentration of the defect is reducing. It suggests a few comments:

a) the peak at 645 cm^{-1} in S_{64} remains at 645 cm^{-1} also in S_{216}, confirming that this mode is very local, with no interaction with the image defects in neighboring cells.

b) Also the intensity remains the same.

c) The A_1 peak at 329 cm^{-1} in S_{64} red shifts to 323 cm^{-1} in S_{216}, indicating that this peak is only marginally dependent on the defect concentration.

d) Its intensity changes a lot: it reduces from about 150 to about 30 km/mol; at high defect dilution this peak is then about 100 times lower than the E dominant peak.

e) With the further dilution of the defect, it is reasonable to expect that its wavenumber will continue to red-shift by 1-2 cm^{-1}, and its intensity to further decrease.

f) In this low region of the spectrum the nitrogen A_1 peak at 323 cm^{-1} is no longer the most intense one, as a peak at 285 cm^{-1} and a second one at 360 cm^{-1} are now emerging, but their intensities are 60 times lower than the dominant one.

We can conclude by saying that the peak at 645 cm^{-1} is the only real defect peak in the spectrum, at least for the experimentally observed N concentrations. Note that its intensity at the S_{216} defect concentration is at least 60 times larger than the one of any other peak. This peak is a clear, dominant fingerprint of the defect.

3.3.2 The VN_x IR spectra.

One can imagine that the presence of the vacancy might change dramatically the IR spectrum with respect to the N_s one, and that the spectrum might change as a consequence of the presence of an increasing number of N atoms. Here we explore the possibility to identify each VNx defect through its IR spectrum, and to differentiate them with respect to the other substitutional N defects.

In the VN_1 and VN_2 cases, as already discussed, two spin states are possible: quadruplet q and doublet d in the first case, and triplet t and singlet s in the second. The low spin states, as shown in Table 1, are by far the more stable. In the left panels of Figure 5 we report the IR spectra of the lowest energy states of the four VN_x defects. The spectra of the high spin states of VN_1 and VN_2 are shown in the Supplementary Material Section (SMS). In the right column of Figure 5, the Raman spectra of VN_x are shown. The symmetry of the high energy q state of VN_1 is C_{3v} (see figure S3 in the SMS, and Table 3 for the wavenumbers and intensities of the most intense peaks) as the three Si atoms around the vacancy have the same spin; under the hypothesis that only the N atom moves (see the discussion of the N_s spectrum), the symmetry of the 3 nitrogen modes is A_1 and E. The A_1 mode, at 339 cm^{-1}, has extremely low intensity (35 km/mol, see first row of Table 3), so that the spectrum is dominated by the E mode at 654 cm^{-1}, whose intensity is 3630 km/mol.

The second spin state of VN_1 is a doublet d, and its symmetry is C_s. The E doubly degenerate mode of q splits into two A modes with a blue shift to 664 and 673 cm^{-1} (see the top left panel of Figure 5), and the intensity is reduced by about a factor 2 (as expected, as the E mode of q is doubly degenerate).

In the high spin VN_2 case (two uncoupled electrons), the symmetry is C_{2v}. Wavenumbers and intensities of the most relevant peaks are reported in Table 3. Only three of them are above the perfect bulk silicon edge at 533 cm^{-1}, and are at 667, 675, 677 cm^{-1}. When a Lorentzian with FWHM of 8 cm^{-1} is used for the convolution of the spectrum, these peaks merge in a single peak centered at 675, with intensity larger than 3000 km/mol (see Figure S2 of the SMS). All other peaks have negligible intensities. The low spin singlet state, the most stable one, is a closed shell, with C_2 symmetry. In this case the three most relevant peaks are separated by about 10 cm^{-1}, with the most intense at 693 cm^{-1}, followed by one at 683 and finally the less intense one at 674

cm^{-1}. So the spectrum of the two spin states differ significantly.
In the VN_3 case there is only one uncoupled electron, so that the ground electronic state is a doublet. The symmetry analysis, using as a basis the Cartesian coordinates of the three N atoms, produces:
$\Gamma^{rid} = 2A_1 + A_2 + 3E$
All these six modes have wavenumbers above the bulk silicon edge; however 3 of them have low, and one null, IR intensity, and are not visible in the spectrum. The most intense modes are listed in Table 3 . They are separated by only 8 cm^{-1}, and merge in a single, extremely intense peak at 695 cm^{-1} .
The VN_4 spectrum is shown in the bottom left panel of figure 4 . Surprisingly enough, also in this case the spectrum reduces to a single peak. In this case the reason is symmetry, as the A_1 (at 546 cm^{-1}), E (at 713 cm^{-1}) and F_1 (701 cm^{-1}) modes are IR inactive. So only three (triply degenerate) F_2 modes are IR active. The first two, however, at 535 and 552 cm^{-1}, have quite low intensity (108 and 39 km/mol). The third one, at 712 cm^{-1}, is extremely intense (14551 km/mol) and fully dominates the spectrum.
In summary, the four VN_x defects in their ground state are dominated by a single (or a couple, or a triplet, but with very close wavenumbers), very intense peak, at about 668 (VN_1), about 690 (VN_2), about 695 (VN_3), and 712 (VN_4) cm^{-1}, so they are well separated from each other (with the exception of VN_2 and VN_3, that differ by only 4 - 8 cm^{-1}), and should be easily visible individually. They are also well separated from N_s (at 645 cm^{-1})

3.3.3 The N_s-N_s and V_2N_2 IR spectra.

One of the most common N substitutional defect is N_s-N_s, in which two vicinal Si atoms are substituted by two N atoms. The IR spectrum (see Figure 6, top) shows exactly the same features as the other five defects discussed above, with a single dominant peak at 678 cm^{-1}, whose intensity is at least 50 times larger than the one of any other peak. This peak falls in between the main peak of VN_1^d (668 cm^{-1}) and that of VN_2^s (690 cm^{-1}); the difference of about 10 cm^{-1} from both should be such to permit to identify the three defects separately; the fact that both VN_1^d and VN_2^s have multiple (although very close) peaks is an additional element for the individual identification of the three defects.
In order to see how vacancy aggregations can change the IR spectrum with respect to other defects, we also modeled a V_2N_2 complex. A second vacancy contiguous to the first one has been generated by eliminating one of the silicon atoms in VN_2. There are then four uncoupled electrons, one around the vacancy with the two N atoms, and three around the other vacancy. The possible spin states are now the singlet ($S_z = 0$), the triplet ($S_z = 1$) and the quintuplet ($S_z = 2$). The singlet turns out to the the most stable state, but the energy of one of the triplets ($V_2N_2^{t1}$ in Table 1) is extremely close to the singlet, as the spin down electron is far from the three spin up (they are around different vacancies). In the second triplet state, the spin down electron is close to two spin up electrons, ($V_2N_2^{t2}$ in Table 1). The quintuplet energy is much higher than the triplet and singlet ones (see Table 3). The comparison of the IR spectrum of the singlet of this defect (see Figure 6, bottom left) with the VN_2 one (Figure 5, second row, left) shows that they are very similar; the additional vacancy changes only marginally the position and intensity of the peaks. The spectrum of the triplet t and of the quintuplet Q are very similar to the one of the singlet s, and are shown in Figure S3 of the SMS.

3.3.4 The Raman spectra

We remind that Raman and IR spectra can differ in two main ways, namely:
a) when symmetry is such that modes are active in IR but not in Raman, or viceversa,
b) also when a mode is active both in IR and Raman, the two intensities can be very different.
Let us consider first the Raman spectrum of N_s (top right panel of Figure 4). It shows that the perfect silicon peak at 533 cm^{-1} just shifts slightly to 535 cm^{-1}; this peak dominates the spectrum of the defective system. The defect peak at 645 cm^{-1} has intensity more than ten times smaller. The one at 329 cm^{-1} disappears in the background. In short, the defective Raman spectrum is not very useful for the identification of this defect. Let us consider now the VN_x series, starting from VN_4, that has T_d symmetry, to which then consideration a) above applies.
The Raman spectrum of VN_4 is shown in the bottom right panel of Figure 5. The A_1, E and F_2 Irreducible Representations of the T_d group are Raman active. There are four well separated high intensity peaks at 474, 535, 552 and 712 cm^{-1}. All of them are of F_2 symmetry (the latter includes also a contribution from an E mode at 713 cm^{-1}).
In the C_{3v} cases (VN_3^d and N_s-N_s defects) the A_1 and E modes are both IR and Raman active, whereas the A_2 modes are only Raman active.
The third panel of the right column of figure 5 refers to VN_3^d, and presents a large peak at 545 cm^{-1} with shoulders at 524 and 530 cm^{-1}, about 11 cm^{-1} above the Raman peak of N_s and 8 cm^{-1} below one of the V_4 peaks. The modes at 687, 694 and 696 cm^{-1} also in this case merge in a single peak, whose intensity is about one quarter of the dominant peak, so that it is still visible. In the N_s-N_s Raman spectrum the main peak is at 539 cm^{-1}; two other peaks, of lower intensity, appear at 473 and 682 cm^{-1}. Also the $V_2N_2^s$ Raman spectrum is dominated by a peak at 540 cm^{-1}, with the defect peaks at about 690 cm^{-1} having much lower intensities.
In summary, the Raman spectra appear not as useful as the IR ones for the characterization and differentiation of the various N substitutional defects. They can, however, provide additional complementary information, in particular in the cases of high symmetry.

4 Discussion and comparison with experiment and previous calculations.

As it has been mentioned in the Introduction, the concentration of nitrogen defects in silicon is usually very low; as a consequence, experimental evidences about these defects are scarce. Implantation techniques permit however to increase dramatically

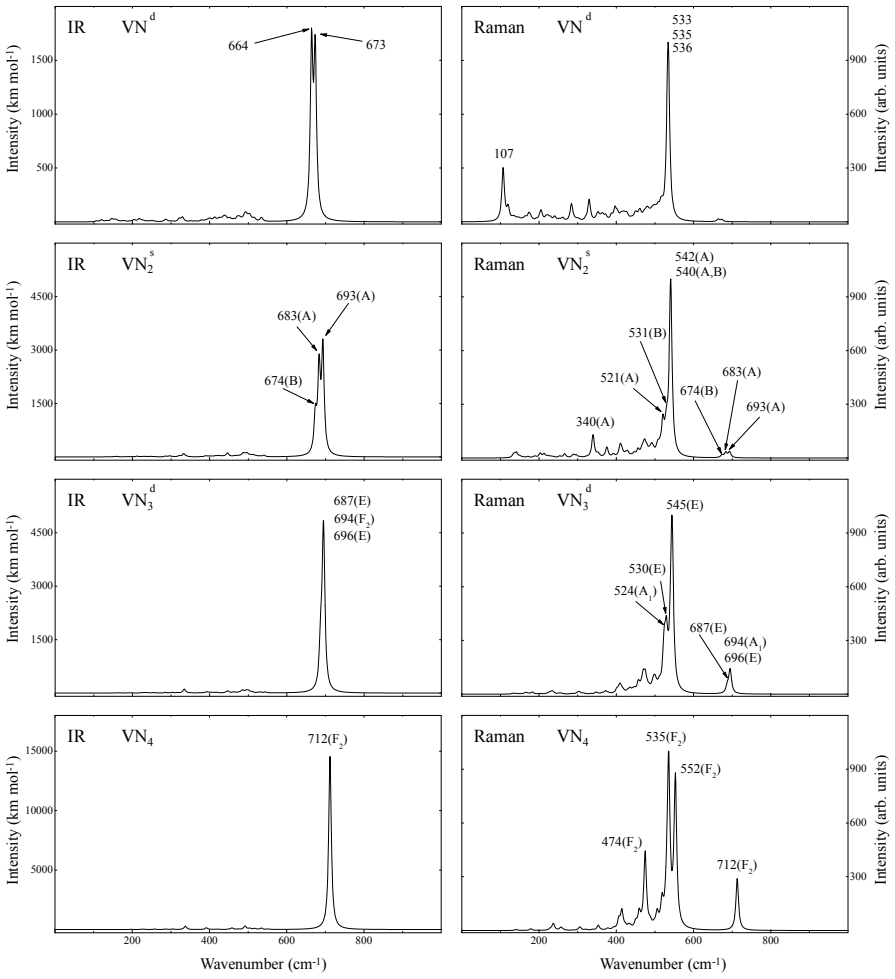

Fig. 5 Left: simulated IR (left) and Raman (right) spectra of VN_x defects in the lowest energy states. Superscripts d and s stand for doublet and singlet. In all cases the S_{64} supercell has been used. In VN^d labels of Irreducible Representations are not reported, as symmetry reduces to C_1.

the concentration of nitrogen in bulk silicon. This is the case of the investigations performed by Stein,[13,14] concerning the IR response of N defects in silicon. Five main peaks at 551, 653, 687, 766 and 963 cm^{-1}, attributed to N defects, have been reported.

Looking at Table 3 and Figures 4, 5 and 6, we try to establish a correspondence between Stein's peaks and our simulated peaks:

a) none of the relevant peaks of the N substitutional defects here investigated is at 551 cm^{-1}. VN_3 has a peak at 545 and VN_4 at 552 cm^{-1}, but their intensity is as small as 43 and 39 km/mol, whereas the dominant peak in the two cases is as high as 4844 and 14551 km/mol. We can conclude that this peak is not due to one of the substitutional defects here investigated.

b) the highest wavenumber peak reported in the table and shown in the three figures just mentioned is at 712 cm^{-1}, so that the two Stein's peaks at 766 and 963 cm^{-1} must be due to interstitial N defects, or more complex (multiple) defects.

c) Stein's peaks at 653 and 687 cm^{-1} are extremely close the the main peak here computed for N_s (at 645 cm^{-1}, 8 cm^{-1} below the experimental peak) and for N_s-N_s (at 685 cm^{-1}, just 2 cm^{-1} below the experiment).

Note however that the present method, with the present basis set and functional, overestimates the Raman active peak of pristine diamond by 12 cm^{-1} (from 521 to 533 cm^{-1}). If we suppose that a similar overestimation is affecting all the computed peaks, we should also explore the windows at 8-16 cm^{-1} above the experimental peaks. The VN_1^d peak at 664 cm^{-1} (11 cm^{-1} above the experiment), with high intensity (1782 km/mol) might be a good candidate, too. Note that in VN_1^d there is a second peak at 673 cm^{-1}, with high intensity (1689 km/mol) that might merge with the previous one to give a single band. The VN_1^q defect presents a peak at 654 cm^{-1}, just 1 cm^{-1} above the experimental peak. It must however be excluded, as the quadruplet q state is about 0.8 eV less stable than the doublet state.

Just above the experimental peak at 687 cm^{-1}, we observe the VN_2^s peak at 693 cm^{-1} (3299 km/mol), and the three peaks of VN_3^q at 687, 694, 696 cm^{-1}, that probably would appear as a single peak, and whose total intensity is as large as 11000 km/mol. VN_2 and VN_3 would require obviously the aggregation of 2 and 3 nitrogen atoms around a vacancy, an event whose

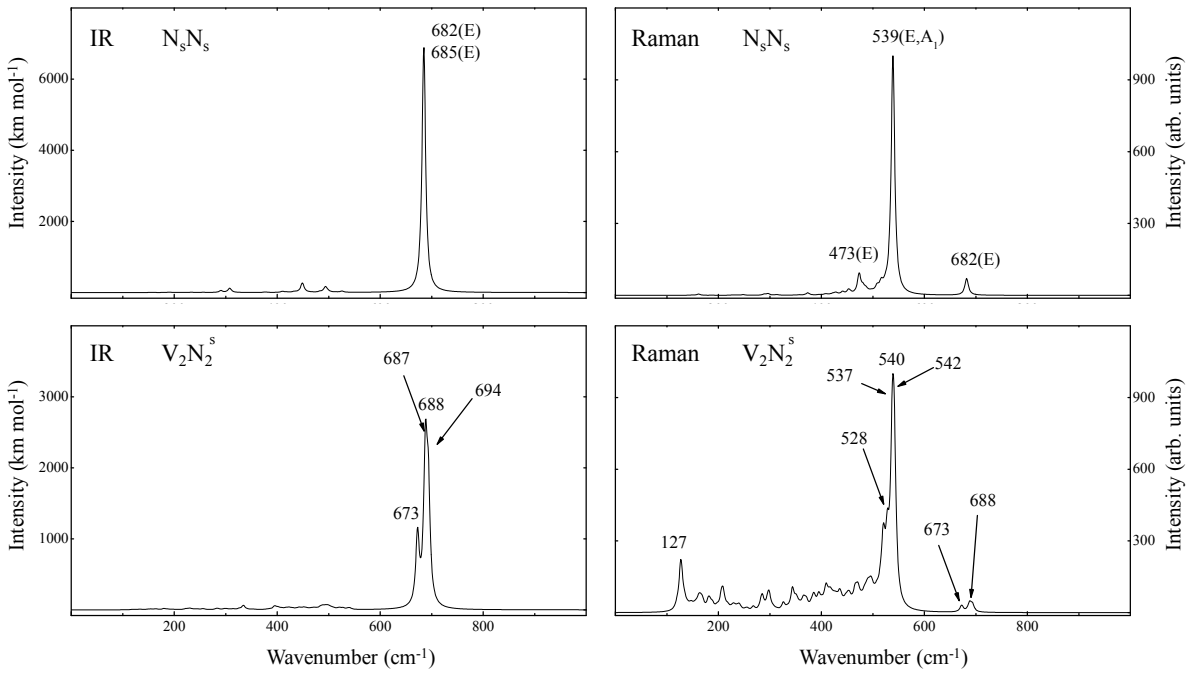

Fig. 6 Top: simulated IR (left) and Raman (right) spectra of N_s-N_s defect. Bottom: simulated IR and Raman spectra of V_2N_2 defect in the singlet state. In all cases the S_{64} supercell has been used.

probability we are unable to estimate.

In 1994 Jones *et al.*[42] computed the vibrational frequency of various defects by using the cluster approach ($N_2Si_{44}H_{42}$) and a LDA type functional, obtaining for N_s 677 cm^{-1} (24 cm^{-1} above the experiment). Nine years later Goss et al.,[15] investigated ten different nitrogen defects in silicon. They used a spin-polarized local-density-functional approach with a Perdew-Wang exchange-correlation functional, the supercell scheme, a Gaussian type basis set for the valence electrons and pseudopotentials for the core ones, and a non-public computer code. Equilibrium geometry, charge and spin density data and the Local Vibrational Modes (LVB) (see ref. 15 for details) of the nitrogen defects were reported. For the single and double nitrogen substitutional defects (N_s and N_s-N_s) they report modes at 637 cm^{-1} (16 cm^{-1} below the experiment) and at 667 cm^{-1} (20 cm^{-1} below the experiment). Note however that they report just the wavenumbers, not the IR intensities, so that the prominent nature of these two peaks can just be guessed. Both Jones *et al.*[42] and Goss et al.[15] report the LVB of defects containing interstitial nitrogen, that we compare with in a parallel paper.[16]

5 Conclusions.

The electronic, structural and vibrational features of seven nitrogen substitutional defects in silicon have been investigated in their neutral states. It is shown that in all cases in which there are two or more possible spin states, the one with the lowest spin multiplicity is the most stable. All systems are characterized by a simple IR spectrum, in which a single peak has intensity at least 20 times larger than any other peak. In some cases the single peak is in fact the superposition of two or three peaks, whose wavenumbers, however, are within a few (maximum 10) cm^{-1}, so that they merge in a single peak, when a Lorentzian with a FWHM as narrow as 8-15 cm^{-1} is used to convolute the spectrum.

These peaks, that can be considered as fingerprints of the various defects, span the 645-712 cm^{-1} interval. The dominant peak is at 645 cm^{-1} for N_s, at 669 for VN_1^d (*d* stands for doublet, the lowest energy spin state), at 684 cm^{-1} for N_s-N_s, at about 688 cm^{-1} for VN_2^s, at 695 for VN_3^d and at 712 cm^{-1} for VN_4^s. The multi-defect system V_2N_2, obtained by adding a second contiguous vacancy to VN_2^s, presents a IR spectrum that essentially coincides with the one of the simpler system, confirming that the characterization of the defect is due to the presence of the N atoms and their position around the (first) vacancy.

The defect Raman spectra are dominated by a single peak, that in all cases is nothing else than a weak perturbation of the pristine silicon peak at 533 cm^{-1} (they span the 520 - 545 cm^{-1} interval). They are then not as useful as the IR spectra for the characterization of the seven defects. However secondary peaks are present in some cases, that can be used as complementary information for differentiating various defects when the IR spectra are not sufficient for reaching this target.

Of the 5 main peaks observed by Stein[13,14] (high N concentration was obtained in this case by using implantation techniques) at 551, 653, 687, 766 and 963 cm^{-1}, only for two it has been possible to find a simulation counterpart. The best candidate for the peak at 653 cm^{-1} is the N_s peak at at 645 cm^{-1}; however, taking into account the usual differences between theory and exper-

iment, the VN_1^d peak at 654 cm^{-1} (very intense: 1782 km/mol) might also be associated to the experimental peak.

The best candidate for the 687 cm^{-1} peak is the N_s-N_s one we compute at 685 cm^{-1}; however the very intense VN_2^s peak at 693 cm^{-1} and VN_3^d at 687 cm^{-1} cannot be ruled out. The above analysis means that the three peaks reported by Stein at 551, 762 and 963 cm^{-1} correspond to interstitial or mixed, or more complicated defects.

In a forthcoming paper,[16] eight such interstitial defects will be explored, to complete the analysis of the possible N defects in silicon, and of their IR and Raman visibility.

ACKNOWLEDGEMENTS

RD and FSG acknowledges the CINECA award (HP10CTG8YY) under the ISCRA initiative, for the availability of high performance computing resources and support.

Notes and references

1 T. Abe and H. Takeno, *MRS Proceedings*, 1992, **262**, 3.

2 T. Sinno, E. Dornberger, W. Von Ammon, R. Brown and F. Dupret, *Mater. Sci. Eng. R Rep.*, 2000, **28**, 149–198.

3 V. Orlov, H. Richter, A. Fischer, J. Reif, T. Müller and R. Wahlich, *Mat. Sci. Semicon. Proc.*, 2002, **5**, 403–407.

4 Q. Sun, K. Yao, H. Gatos and J. Lagowski, *J. Appl. Phys.*, 1992, **71**, 3760–3765.

5 C. R. Alpass, J. D. Murphy, R. J. Falster and P. R. Wilshaw, *J. Appl. Phys.*, 2009, **105**, 013519.

6 C. Ewels, R. Jones, S. Öberg, J. Miro and P. Deak, *Phys. Rev. Lett.*, 1996, **77**, 865.

7 M. Tajima, T. Masui, T. Abe and T. Nozaki, *Jap. J. Appl. Phys.*, 1981, **20**, L423.

8 R. Sauer, J. Weber and W. Zulehner, *Appl. Phys. Lett.*, 1984, **44**, 440–442.

9 X. Dong, N. Li, C. Liang, H. Sun, G. Feng, Z. Zhu, H. Shao, X. Rong, L. Zhao and J. Zhuang, *Appl. Phys. Expr.*, 2013, **6**, 081301.

10 D. Xiao, L. Ning, Z. Zhen, S. Hezhu, R. Ximing, L. Cong, S. Haibin, F. Guojin, Z. Li and Z. Jun, *Appl. Phys. Lett.*, 2014, **104**, 091907.

11 Y. Itoh, T. Nozaki, T. Masui and T. Abe, *Appl. Phys. Lett.*, 1985, **47**, 488–489.

12 K. L. Brower, *Phys. Rev. Lett.*, 1980, **44**, 1627.

13 H. Stein, *Appl. Phys. Lett.*, 1983, **43**, 296–298.

14 H. Stein, *Appl. Phys. Lett.*, 1985, **47**, 1339–1341.

15 J. Goss, I. Hahn, R. Jones, P. Briddon and S. Öberg, *Phys. Rev. B*, 2003, **67**, 045206.

16 A. Platonenko, F. S. Gentile, J. Maul, F. Pascale, E. A. Kotomin and R. Dovesi, *Mater. Today Comm.*, 2019.

17 A. D. Becke, *J. Chem. Phys.*, 1993, **98**, 5648–5652.

18 C. Lee, W. Yang and R. Parr, *Phys. Rev. B*, 1988, **37**, 785–789.

19 R. Dovesi, R. Orlando, A. Erba, C. M. Zicovich-Wilson, B. Civalleri, S. Casassa, L. Maschio, M. Ferrabone, M. D. L. Pierre, P. D'Arco, Y. Noël, M. Causà, M. Rérat and B. Kirtman, *Int. J. Quantum Chem.*, 2014, **114**, 1287.

20 J. S. Binkley, J. A. Pople and W. J. Hehre, *J. Am. Chem. Soc.*, 1980, **102**, 939–947.

21 P. D'Arco, G. Sandrone, R. Dovesi, R. Orlando and V. Saunders, *Phys. Chem. Mineral*, 1993, **20**, 407–414.

22 M. M. Francl, W. J. Petro, W. J. Hehre, J. S. Binkley, M. S. Gordon, D. J. DeFrees and J. A. Pople, *J. Chem. Phys.*, 1982, **77**, 3654–3665.

23 R. Dovesi, V. R. Saunders, C. Roetti, R. Orlando, C. M. Zicovich-Wilson, F. Pascale, B. Civalleri, K. Doll, N. M. Harrison, I. J. Bush, P. D'Arco and M. Llunell, *CRYSTAL 2014 User's Manual*, University of Torino, Torino, 2013.

24 F. Pascale, C. M. Zicovich-Wilson, F. L. Gejo, B. Civalleri, R. Orlando and R. Dovesi, *J. Comput. Chem.*, 2004, **25**, 888–897.

25 C. M. Zicovich-Wilson, F. Pascale, C. Roetti, V. R. Saunders, R. Orlando and R. Dovesi, *J. Comput. Chem.*, 2004, **25**, 1873–1881.

26 A. Erba, M. Ferrabone, R. Orlando and R. Dovesi, *J. Comput. Chem.*, 2013, **34**, 346–354.

27 C. Carteret, M. De La Pierre, M. Dossot, F. Pascale, A. Erba and R. Dovesi, *J. Chem. Phys.*, 2013, **138**, 014201.

28 J. Baima, M. Ferrabone, R. Orlando, A. Erba and R. Dovesi, *Phys. Chem. Minerals*, 2016, **43**, 137–149.

29 F. Pascale, C. M. Zicovich-Wilson, R. Orlando, C. Roetti, P. Ugliengo and R. Dovesi, *J. Phys. Chem. B*, 2005, **109**, 6146–6152.

30 G. M. Barrow, *Introduction to Molecular Spectroscopy*, McGraw-Hill, New York, 1962, p. 70.

31 B. A. Hess, L. J. Schaad, P. Carsky and R. Zahradnik, *Chem. Rev.*, 1986, **86**, 709–730.

32 L. Maschio, B. Kirtman, R. Orlando and M. Rérat, *J. Chem. Phys.*, 2012, **137**, 204113.

33 L. Maschio, B. Kirtman, M. Rérat, R. Orlando and R. Dovesi, *J. Chem. Phys.*, 2013, **139**, 167101.

34 L. Maschio, B. Kirtman, M. Rérat, R. Orlando and R. Dovesi, *J. Chem. Phys.*, 2013, **139**, 164101.

35 L. Maschio, B. Kirtman, M. Rérat, R. Orlando and R. Dovesi, *J. Chem. Phys.*, 2013, **139**, 164102.

36 M. Ferrero, M. Rérat, R. Orlando and R. Dovesi, *J. Comput. Chem.*, 2008, **29**, 1450–1459.

37 M. Ferrero, M. Rérat, R. Orlando and R. Dovesi, *J. Chem. Phys.*, 2008, **128**, 014110.

38 K. L. Brower, *Phys. Rev. B*, 1982, **26**, 6040–6052.

39 S. F. Boys and F. Bernardi, *Mol. Phys.*, 1970, **19**, 553–566.

40 N. Fukata, A. Kasuya and M. Suezawa, *Jap. J. Appl. Phys.*, 2001, **40**, L854.

41 J. H. Parker, D. W. Feldman and M. Ashkin, *Phys. Rev.*, 1967, **155**, 712–714.

42 R. Jones, S. Öberg, F. B. Rasmussen and B. B. Nielsen, *Phys. Rev. Lett.*, 1994, **72**, 1882.

Institute of Solid State Physics, University of Latvia as the Center of Excellence has received funding from the European Union's Horizon 2020 Framework Programme H2020-WIDESPREAD-01-2016-2017-TeamingPhase2 under grant agreement No. 739508, project CAMART²